

# PERIDYNAMIC SIMULATION PLATFORM TO DETERMINE VIRTUAL ALLOWABLES OF MANUFACTURING DEVIATIONS

Christian Willberg, Jan-Timo Hesse & Daniel Krause

Institute for Composite Structures and Adaptive Systems, German Aerospace Center

## Abstract

In this paper a Peridynamics based simulation platform is reported. The framework enables the analysis of structure and fracture mechanical problems. For such a platform, a number of things have to be taken into account. Flexible material modeling should be possible. Furthermore, geometric models must be easy to integrate. An interface for existing material models has been integrated. It is based on the Abaqus UMAT quasi standard and allows the use of existing Fortran routines. For the geometry modeling, the input of the Peridynamics software Peridigm was extended. It allows now the flexible use of arbitrary geometries and local coordinate systems. Because one application of such platform is the determination of virtual allowables, several standard tests are implemented as well. These models are parametrized and allow flexibility within the specific standard. The whole software framework is structured with a loose coupling. Therefore, software tools for model generation, analysis and export can be easily separated and exchanged by other software. In this paper the whole framework and as an example its use for the calculation for allowables is illustrated. From a practical point of view some ideas for usability are given, e.g. different level of user entrance complexity (GUI, API and open source).

**Keywords:** Peridynamics, Composites, Fatigue, Digitalization, Framework

## 1. Introduction

For the analysis of complex and large scale structural mechanical problems, simulations on all levels of the aircraft design process and efficient simulation frameworks are required. Methods of digitalization are to be highlighted. A software should not be encapsulated as a single tool. The interaction and communication of several tools and modules is essential and brings many benefits. If properly designed no additional wrappers are needed between interfaces. The advantages are that specialists can focus on their area of expertise and the software components can be used more broadly.

A Peridynamics based simulation platform is presenting addressing this needs. The framework enables the analysis of structure and fracture mechanical problems and can be used, for example, to determine simulation-based allowables. The underlying peridynamic theory has many advantages and has great potential [1, 2]. It is a non-local method which overcomes discontinuity problems of the classical continuum mechanics theory, which is the basis for the finite element method in structural engineering. On the contrary to continuum mechanics an integral formulation is used instead of a differential one, to formulate the conservation of momentum, angular momentum and energy. As a result, in the original peridynamic formulation the material models have to be rewritten [3]. To avoid this and to improve the applicability of the peridynamic theory, the so-called correspondence formulation (motivated by the correspondence principle of Nils Bohr [4]) was developed by Stuart Silling [5] in 2007. This formulation introduces a non-local integral deformation gradient, which allows the use of classical continuum mechanics models in Peridynamics. The advantage of such existing models is that, already validated material models can be used.

The focus is then to use the improved fracture mechanics modeling to support experiments. The focus is to create virtual allowables [6] and in the analyses of undulations as they occur in automated

fiber placement processes [7]. Within the proposed peridynamic framework virtual experiments are used to calibrate and validate the damage model with GIC and GIIIC virtual experiment. For that parametrized model generators are used and loosely coupled with the peridynamic analysis core. Within the framework this is done via APIs by creating the models directly within another tools. Since these tools are focused on FEM, the analysis core communicates via APIs with a wrapper tool. This tool enables the conversion of FEM models into different FEM tool input decks and the peridynamic data set. This API strategy allows for tool reuse and expansion of the user base. Finally, the validated damage model is then used to analyze undulations.

Within this paper this concept and results are shown. It starts with the peridynamic theory. In a next part the framework, its interface definitions and the introduction of external material models is shown. Based on that, different experiments and some results are shown, discussed and is finally concluded.

## 2. Theoretical background

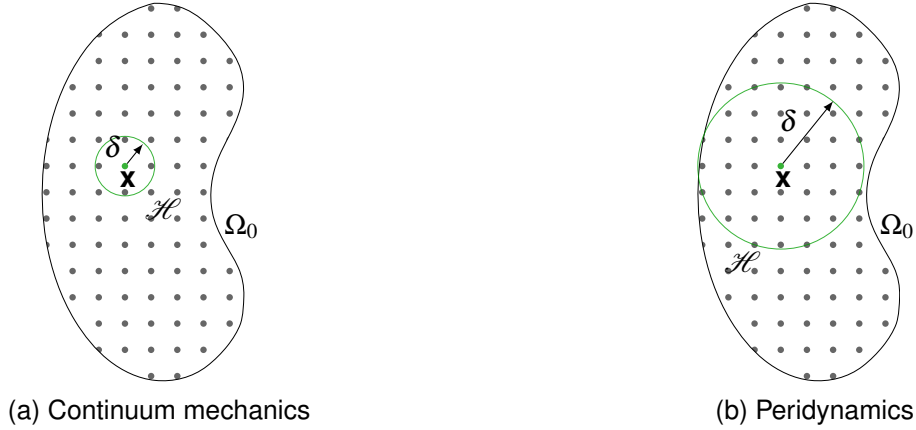


Figure 1 – Interaction domains

As stated before Peridynamics is a non-local theory. The difference between the local continuum mechanics and the Peridynamics theory is illustrated Figures 1a and 1b. A point  $\mathbf{x}$  in a domain  $\Omega_0$  interacts within a subdomain or neighborhood  $\mathcal{H}$  with a specific radius  $\delta$ . For classical continuum mechanics  $\delta \rightarrow 0$ . The paper follows the assumptions and notations made by Silling et al. [5]. Here, within a neighborhood  $\mathcal{H}$ , with the volume  $V_{\mathbf{x}}$ , defined by a spherical domain with the horizon  $\delta$ , the force volume density state  $\underline{\mathbf{T}}$  for a bond interaction between the positions  $\mathbf{x}$  and  $\mathbf{x}'$  is defined as the integral balance of momentum as

$$\int_{\mathcal{H}} (\underline{\mathbf{T}}(\mathbf{x}, t) \langle \mathbf{x}' - \mathbf{x} \rangle - \underline{\mathbf{T}}(\mathbf{x}', t) \langle \mathbf{x} - \mathbf{x}' \rangle) dV_{\mathbf{x}} + \mathbf{b} = \rho \ddot{\mathbf{u}}. \quad (1)$$

Dependent on the assumptions  $\underline{\mathbf{T}}(\mathbf{x}, t) \langle \mathbf{x}' - \mathbf{x} \rangle$  and  $\underline{\mathbf{T}}(\mathbf{x}', t) \langle \mathbf{x} - \mathbf{x}' \rangle$  could have the same orientation and amplitude (bond-based), same orientation, but different amplitude (ordinary state-based) or the orientation and amplitude are different. The latter one called non-ordinary state-based formulation and is shown in Figure 2. It is used for the correspondence formulation. Within the three variations of the peridynamic model, the bond-based, the ordinary state-based and the non-ordinary state-based formulation, flexibility increases, but so does the complexity of the formulations.

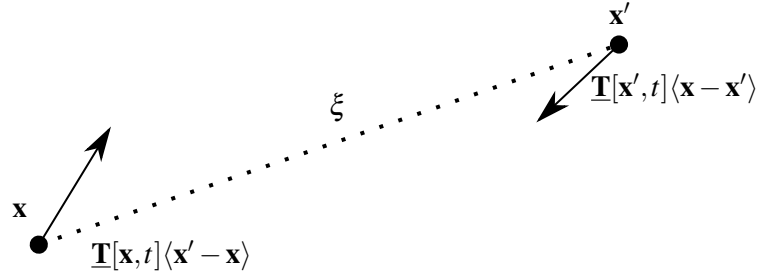


Figure 2 – Illustration of non-ordinary state-based forces used for the correspondence formulation.

## 2.1 Material model

A special formulation of the non-ordinary state-based model was introduced by Silling et al. [5] in 2007. This so-called “correspondence” formulation defines an integral non-local deformation gradient

$$\mathbf{F} = \left[ \int_{\mathcal{H}} \underline{\omega}(\xi) \underline{\mathbf{Y}}(\xi) \otimes \underline{\mathbf{X}}(\xi) dV_{\mathbf{x}} \xi \right] \cdot \mathbf{K}^{-1} \quad (2)$$

to calculate the bond force vector density states, where

$$\mathbf{K} = \int_{\mathcal{H}} \underline{\omega}(\xi) \underline{\mathbf{X}}(\xi) \otimes \underline{\mathbf{X}}(\xi) dV_{\mathbf{x}} \quad (3)$$

is the shape tensor with  $V_{\mathbf{x}}$  defined as the neighborhood volume. For each bond  $\xi$ , there is an influence function  $\underline{\omega}(\xi)$ , an undeformed vector state  $\underline{\mathbf{X}}(\xi)$  and a deformed vector state  $\underline{\mathbf{Y}}(\xi)$ . The shape tensor has to be positive definite and symmetric. The advantage using the non-local deformation gradient is that classical continuum mechanical models can be applied in Peridynamics. The peridynamic force density vector state is

$$\underline{\mathbf{T}}(\xi) = \underline{\omega}(\xi) \mathbf{P} \mathbf{K}^{-1} \xi. \quad (4)$$

The Piola-Kirchhoff stress tensor [8] with respect to an orthonormal basis can be determined as

$$\mathbf{P} = \det \mathbf{F} \boldsymbol{\sigma} \mathbf{F}^{-1}. \quad (5)$$

For an arbitrary material the Cauchy stresses  $\boldsymbol{\sigma}$  in local coordinates have to be determined. As one example the Green-Lagrange strain tensor [8] is used as a strain measure

$$\boldsymbol{\varepsilon} = \frac{1}{2} (\mathbf{F}^T \mathbf{F} - \mathbf{I}). \quad (6)$$

to determine the global Cauchy stresses as

$$\boldsymbol{\sigma} = \mathbf{R} \frac{\partial \boldsymbol{\sigma}_{local}}{\partial \boldsymbol{\varepsilon}_{local}} \mathbf{R}^T \boldsymbol{\varepsilon} \mathbf{R} \mathbf{R}^T. \quad (7)$$

with  $\mathbf{R}$  as rotation matrix to transform local coordinates to global ones.

For a discretized form of correspondence models, the so called zero-energy modes could occur [9]. These modes are non-physical and lead to unstable or unreasonable solutions. One reason is, that the same integral deformation gradient can be calculated by various point distributions. As a result points could “jump” in a new position without the need of a force or energy, without violating the integral conservation rules. Several stabilization methods were published to overcome this problem [10, 11, 12, 13, 14, 15]. A promising approach was published by Wan et al. in 2019 [16]. Instead of a bond-based stabilization method proposed by Silling [17], Wan et al. developed a state-based stabilization method. As positive side effect this method stabilizes the solution for anisotropic material as well. The corrected force density state  $\underline{\mathbf{T}}^C$  with suppression of the zero-energy mode is

$$\underline{\mathbf{T}}^C = \underline{\mathbf{T}} + \underline{\mathbf{T}}^S, \quad (8)$$

where  $\underline{\mathbf{T}}$  is given in Equation 4. Following Wan et al. [16] the suppression force density state  $\underline{\mathbf{T}}^S$  is

$$\underline{\mathbf{T}}^S\langle\xi\rangle = \underline{\omega}\langle\xi\rangle \mathbf{C}_1 \underline{\mathbf{z}}. \quad (9)$$

with  $\underline{\mathbf{z}}$  as the non-uniform deformation state

$$\underline{\mathbf{z}}\langle\xi\rangle = \underline{\mathbf{Y}}\langle\xi\rangle - \mathbf{F}\xi \quad (10)$$

caused by the zero-energy mode. If the approximated non-local deformation gradient  $\mathbf{F}$  exactly maps each undeformed bond to the deformed configuration no zero-energy mode occur. In that case the non-uniform deformation state is zero and the corrected force density state  $\underline{\mathbf{T}}^C$  is equal to the force density state  $\underline{\mathbf{T}}$ . The second order tensor  $\mathbf{C}_1$  is given as

$$\mathbf{C}_1 = \mathbf{C}\mathbf{K}^{-1}, \quad (11)$$

e.g. utilizing the elasticity tensor from Hook's law.

## 2.2 Damage model

An energy based damage model has been utilized [18]. This model is superior to the widely used and simple to implement critical stretch model. The reason is that the critical stretch cannot be determined experimentally. The change in distance between two points does not say anything about how it is achieved. This becomes clear when decomposing into a dilatoric and a deviatoric part as it is done typically for isotropic materials. The fracture energy of a material is equal. The critical stretch for a shear dominated load case is different from a tension dominated load case. Hence, the same fracture energy can be generated by different critical stretches. As a result, the critical stretch fitted to the energy release rate does not reproduce the characteristic value in a virtual experiment. Following Foster et al. [18] for the correspondence material the bond energy density is

$$w_{bond} = (\underline{\mathbf{T}}^P(\mathbf{x}, t)\langle\mathbf{x}' - \mathbf{x}\rangle - \underline{\mathbf{T}}^P(\mathbf{x}', t)\langle\mathbf{x} - \mathbf{x}'\rangle) \cdot \underline{\boldsymbol{\eta}} \quad (12)$$

where the projected force density state  $\underline{\mathbf{T}}^P$  is given by projecting the corrected force vector states  $\underline{\mathbf{T}}^C$  onto the relative displacement with state  $\underline{\boldsymbol{\eta}}$

$$\underline{\mathbf{T}}^P = \frac{\underline{\mathbf{T}}^C \cdot \underline{\boldsymbol{\eta}}}{|\underline{\boldsymbol{\eta}}|}. \quad (13)$$

The decomposition in different energy states, i.e. a dilatoric and a deviatoric part, can be done by decomposing the Cauchy stresses Equation 7 and the Green Lagrange strain tensor Equation 6. In this paper the decomposition has not been analyzed.

A bond fails if it exceeds a specific critical energy  $w_c$ . Foster et al. [18] derived a maximum elastic bond potential value  $w_c$ . This value is based on the energy release rate  $G_0$  and the horizon  $\delta$ . The elastic bond potential is given in Equation 14 (a) for three-dimensional and Equation 14 (b) for the two-dimensional case with thickness  $h$ .

$$w_c = \frac{4G_0}{\pi\delta^4} \quad (a) \quad w_c = \frac{3G_0}{\pi\delta^3 h} \quad (b) \quad (14)$$

This criterion does not differ between traction and compression. In this paper this formulation is adopted. Only bonds with positive stretch  $|\underline{\mathbf{Y}}\langle\xi\rangle| - |\underline{\mathbf{X}}\langle\xi\rangle| > 0$  are analyzed whether the critical energy  $w_c$  is reached or not. The whole theory is implemented in the Peridigm framework [19]. The analysis in this paper is done using a Verlet time-integration schema. The whole solving process is sketched in Willberg et al. [20] in "Section 4 Implementation".

## 3. Implementation

The framework is shown in Figure 3. The framework is designed for flexibility and usability. The user can chose to interact with the framework with mobile devices, scripts or desktop PCs directly. The framework can be controlled via script, API or in a limited way with a graphical user interface. Especially, the APIs allow the user to use each component separately. This is helpful, if the framework should be integrated in other processes.

## PERIDYNAMIC SIMULATION PLATFORM TO DETERMINE VIRTUAL ALLOWABLES

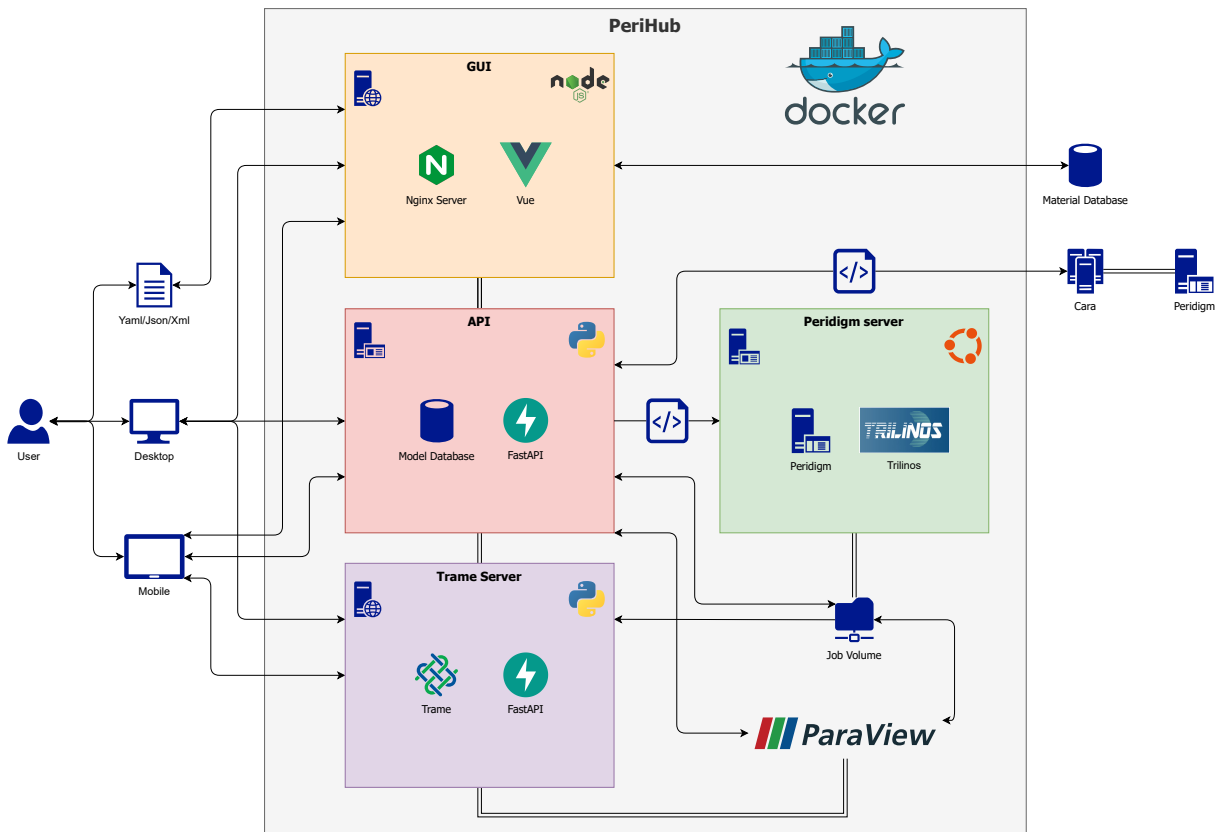


Figure 3 – Framework.

If the process is started a model has to be generated. This is done using already existing model generators. They create virtual experiments to determine virtual allowables. If needed, the model generation process can be coupled with uncertainty or sensitivity analysis [21]. The models are then used in the Peridynamic tool Peridigm. This software uses a mesh free method for the numerical solving process and has been expanded in several ways. E.g. local coordinates for each point has been included as well as a material model interface. In the field of material modeling, the finite element software Abaqus is typically used. This software allows the use of so-called user materials (UMAT). UMATs are written in Fortran and apart from the fact that there are alternatives, it is the quasi-standard in this research area. The proposed interface allows direct interaction between Peridigm and Abaqus UMAT. This reduces the hurdle of material modeling in Peridynamics and gives researchers the full advantage of the Peridigm framework. To include a user material, the architecture of Peridigm was extended as shown in Figure 4. The user material can be included as a normal correspondence material. Oriented at the Abaqus quasi standard an arbitrary number of properties can be defined. This is then parsed in the material routine. For Peridigm the whole setup had to be restructured. The strains are transformed in local coordinates. In this coordinate system the stresses are determined for each neighborhood. This is done by calling the `user_material_interface_correspondence`. The key here is that this interface calls an already pre-compiled Fortran routine which calls then a pre-compiled UMAT. Since the material name is not directly transferable from C++ to Fortran, this additional small Fortran routine was inserted. This routine converts the string definition of C++ into the character field definition of Fortran. By doing so, the pre-compiled UMAT library can be exchanged, by overwriting the existing one. A separation of material is done by material names and checks within the UMAT. This is similar to the Abaqus quasi-standard. The UMAT interface shown Figure 4 is not fully supported by Peridigm. The reason is that some of the parameters are not needed outside the Abaqus finite element environment.

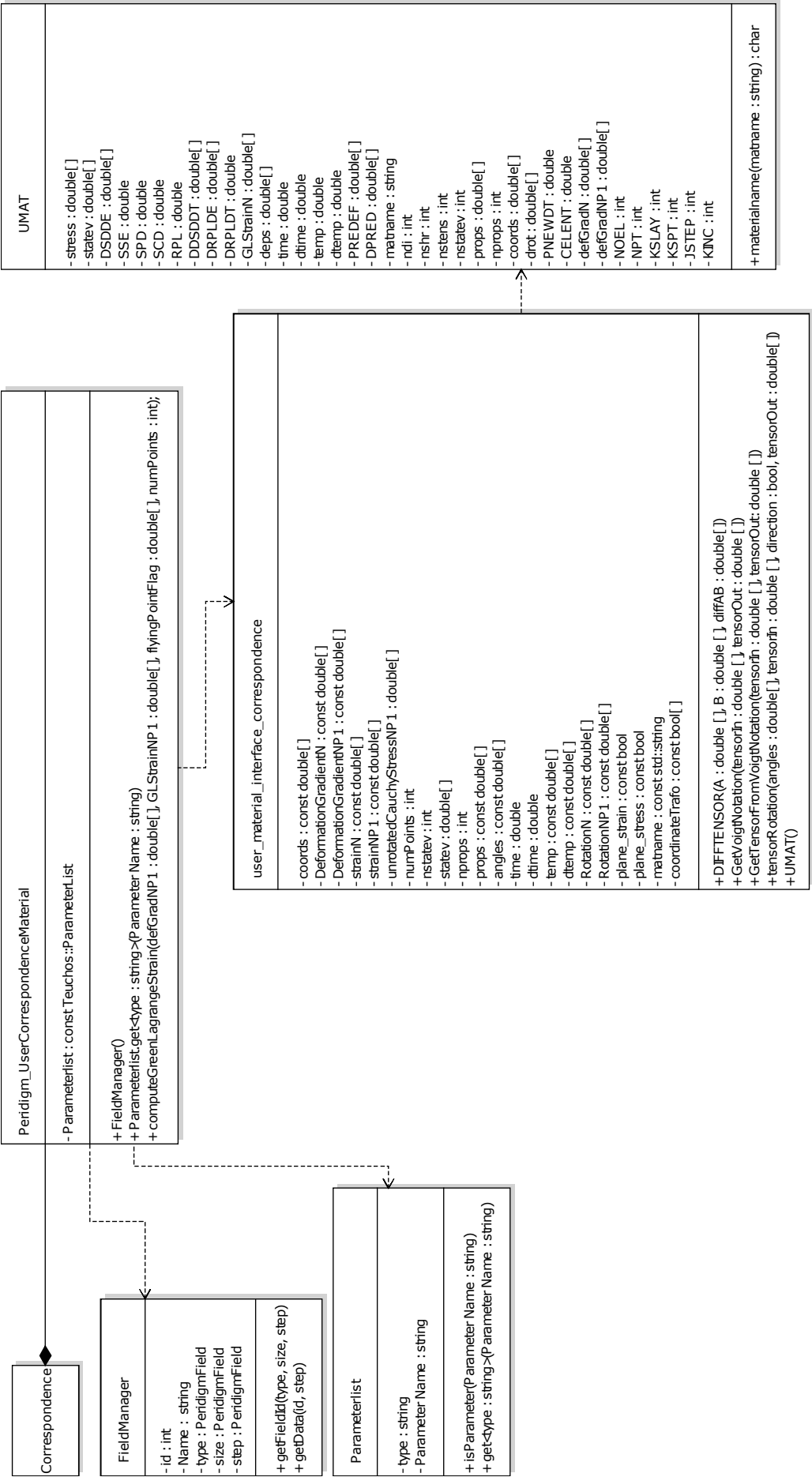


Figure 4 – UML schema.

The presented software material software interface is structured in such a way that other material models and languages can be added easily. The added interface layer must be adapted in that case. The interface supports a user-defined number of status variables. These variables can be exported in the output as well and visualized in the post-processing.

After running the model the results are provided in a Exodus binary file based on the HDF5 standard. This file is readable by the open source software ParaView. All predefined state variables can be selected and shown in ParaView. Moreover, scripts can be used via APIs to extract specific information from the HDF5 file, e.g. the calculation of the energy release rate based on the force-displacement curve or the extraction of curves and the export in other data formats.

#### 4. Application

The section is intended to clarify the concept of virtual allowable prediction. The fracture mode I characteristic value  $G_{IC}$  is determined with a real experiment. This is then recalculated in a virtual experiment and fitted if necessary. The  $G_{IIC}$  value is then determined in the simulation model and validated with experiments. If this works the transfer of the determined characteristic values takes place. The example presented later is a undulation test. This can be validated if necessary. The idea is that more variants can be considered through the automated modeling.

##### 4.1 $G_{IC}$ model

Based on the ASTM E647-00 standard [20], the homogenous isotropic compact tension specimen is shown in Figure 5. It is used to calculate the mode I energy release rate  $G_{IC}$ , Equation 15. The tension loaded specimen is prepared with a notch and an initial crack on the left side. With increasing load, the crack propagates further to the right side. After the simulation is completed, the results can be automatically read and evaluated within the rest API. For an exact measurement of the crack length, the damaged nodes are localized and the exact crack curve can be determined with the help of a weighted polynomial regression. If the crack length  $a_{crack}$  and the dissipated energy  $W_{diss}$  are determined, the energy release rate  $G_{IC}$  can be calculated as follows:

$$G_{IC} = \frac{W_{diss}}{Ba_{crack}}, \quad (15)$$

where  $B$  is the width of the specimen. For brittle material the dissipated energy can be determined by subtracting the linear elastic part from the integral of the load-displacement curve as

$$W_{diss} = \int_0^{u_{max}} F(u) - F_{linear}(u) du. \quad (16)$$

The fracture toughness  $K_{IC}$  is not needed for the used damage model shown in subsection 2.2 If it is needed for plane stress conditions it can be calculated with the Young's modulus  $E$  as [21]

$$K_{IC} = EG_{IC}. \quad (17)$$

The resulting load displacement curve can be seen in Figure 6. At a displacement of  $0.016m$  the load  $F_y$  is constantly decreasing due to the propagating crack.



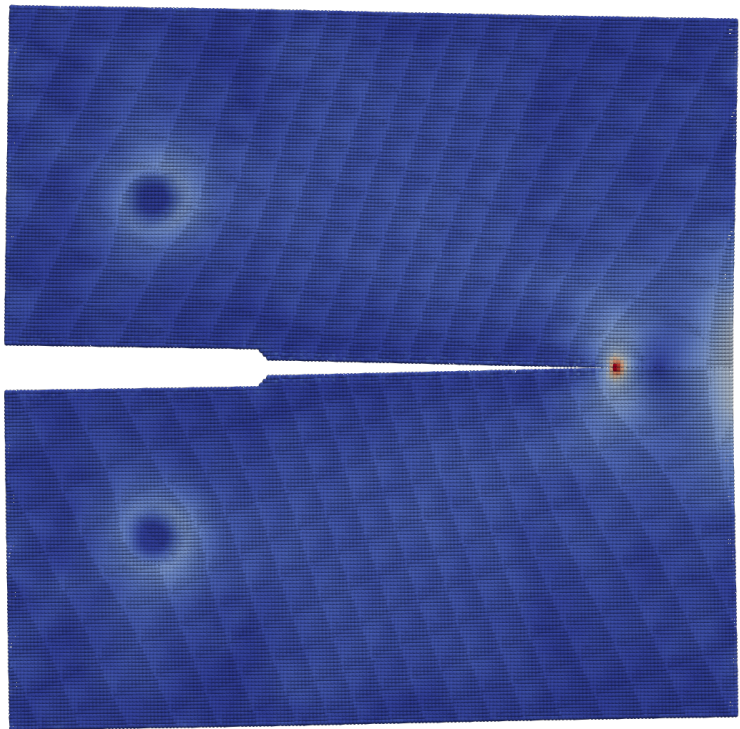


Figure 5 – Numerical results of stresses of a compact tension model.

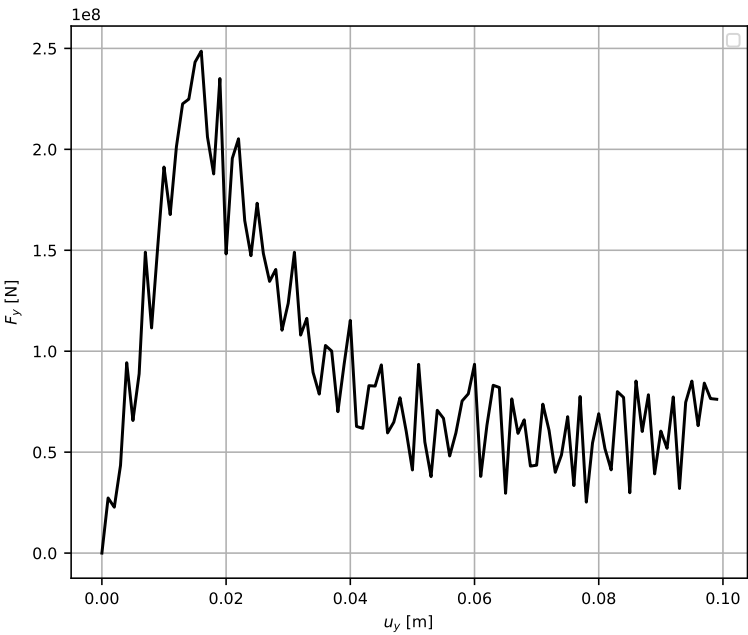


Figure 6 – Load Displacement curve of a compact tension model.



#### 4.2 $G_{IIC}$ model

For the second example the ASTM D7905M-14 standard [22] is utilized. The specimen is placed on two roller bearings and is loaded in the middle with an increasing force. Several features have been implemented to map an unidirectional laminate. For example, the interface between the upper and lower layer needs to be defined, in that way the energy release rate for different sections of the model can be adjusted by the user. Besides that, the fibre orientation of each node can be changed. Thus, the three-point bending test can be simulated with various composite materials. The initial delamination needed for the experiment, with the length  $a$ , is added on the left side via a bond filter. As can be seen in Figure 7, the crack will propagate along the layer interfaces to the right side. When the crack begins to extend itself the corresponding critical load  $P$  and displacement of the crosshead  $d$  is measured and  $G_{IIC}$  will be calculated:

$$G_{IIC} = \frac{9P \cdot a^2 1000d}{2B(\frac{1}{4}L^3 + 3a^3)} \quad (18)$$

$B$  is the width of the specimen and  $L$  is the span length between both bearings.

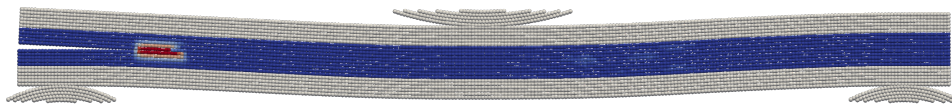


Figure 7 – Numerical results of the damage index in an multilayer laminate specimen as a result of three point bending.

#### 4.3 Undulation model

The production processes of fibre composites can lead to manufacturing induced deviations. A typical deviation is fibre waviness [7]. In Figure 8 the failure pattern of a specimen under compressive load with undulated fibres is shown. Fibre undulation leads to a local decrease in stiffness and strength [23]. A simplified model with a sinussoidal fibre orientation for peridynamic was created. Anisotropic material and material coordinate systems [24] are required for the execution of the undulation models. This material was incorporated via the user material interface. The energy-based damage model was used for damage modeling. Analyzing this model for compressive load leads to Figure 9. It can be seen that for homogenized material the crack propagates in a similar fashion like the experiment. This first test shows, that the peridynamic framework is generally capable of modeling the behavior accurately.

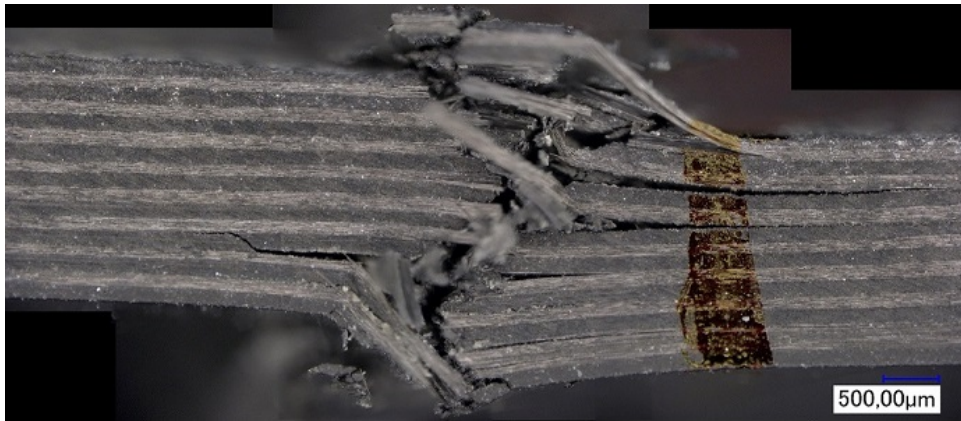


Figure 8 – Fracture of an UD laminate specimen with undulations under pressure load.

In Figure 10 damage indices of a multilayered specimen with undulations can be seen. The relating model was dynamically generated, simulated and analyzed through the framework. Due to the introduced defects of the sample, the reduced stiffness can be summarized in so-called knock-down-factors (KDF). With the help of the presented framework it is possible to determine such KDFs

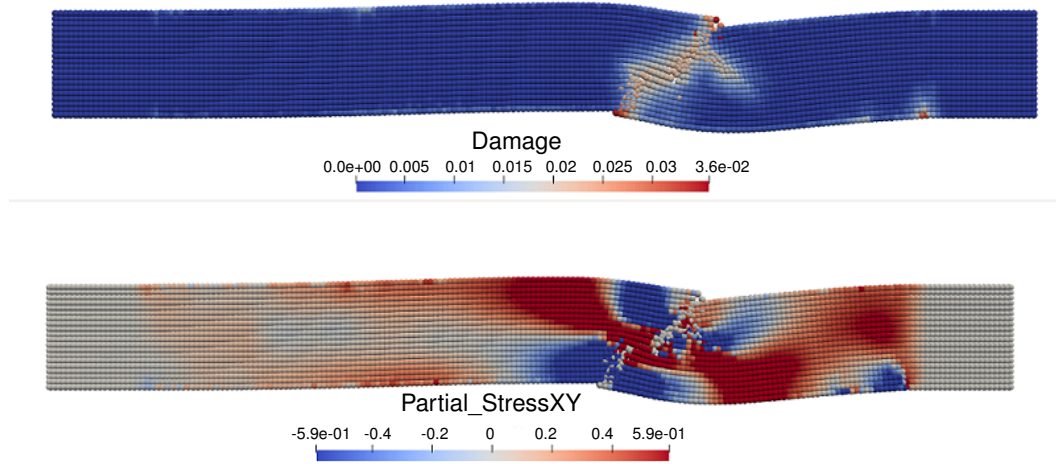


Figure 9 – Numerical results an UD laminate specimen with undulations under pressure load.

automatically and to use them for different design steps. For further probabilistic analysis of various geometries the framework is able to aid for an efficient and sustainable simulation entrypoint.

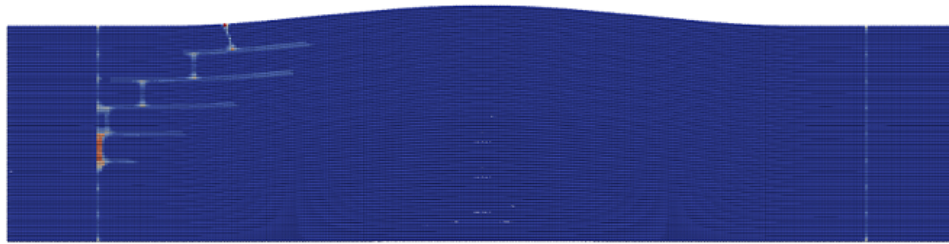


Figure 10 – Numerical results of the damage index in an multilayer laminate specimen with undulations under pressure load.

## 5. Conclusion

In the paper a peridynamic simulation framework has been shown. Initially the used peridynamic simulation methods, corresponding material and damage models were introduced. Due to the limitations of the current available peridynamic simulation platforms the need of an user friendly framework was highlighted. The framework includes interfaces to various model generators as well as an UMAT interface. It allows the flexible determination of virtual allowables. Because of the different usage possibilities (Code, API, GUI) the user has several entry levels. This allows him to use the framework as needed and does not have to learn everything in detail. This way of providing framework availability helps by the dissemination.

Besides the relevant Implementations, the modeling of several virtual experiments was shown. It can be seen, that for the more complex undulation problem the failure mode can be reproduced. In future work, the framework has to be extended. Because in typical manufacturing deviations multilayer composites with no uniform orientation has to be considered. An example for that is shown in Figure 10. Further delaminations can be observed here and the effects to the virtual allowables have to be analyzed. Additionally, the framework and its components have to be validated and benchmarked to other modeling tools.

## 6. Contact Author Email Address

Christian Willberg, <mailto:christian.willberg@dlr.de>  
 Jan-Timo Hesse, <mailto:jan-timo.hesse@dlr.de>

Daniel Krause, mailto: daniel.krause@dlr.de

## 7. Copyright Statement

The authors confirm that they, and/or their company or organization, hold copyright on all of the original material included in this paper. The authors also confirm that they have obtained permission, from the copyright holder of any third party material included in this paper, to publish it as part of their paper. The authors confirm that they give permission, or have obtained permission from the copyright holder of this paper, for the publication and distribution of this paper as part of the ICAS proceedings or as individual off-prints from the proceedings.

## References

- [1] Dias J P, Bazani M A, Paschoalini A T and Barbanti L. *A Review of Crack Propagation Modeling Using Peridynamics*, pp 111–126. Springer International Publishing, Cham. 2017.
- [2] Javili A, Morasata R, Oterkus E and Oterkus S. Peridynamics review. *Mathematics and Mechanics of Solids*. 2018.
- [3] Silling S A. Reformulation of elasticity theory for discontinuities and long-range forces. *Journal of the Mechanics and Physics of Solids*, Vol. 48, No. 1, pp 175–209. 2000.
- [4] Bohr N. *The Correspondence Principle 1918-1923*, Vol. 3 of *Niels Bohr Collected Works*. North-Holland Publishing Company, Amsterdam, New York, Oxford. 1976.
- [5] Silling S A, Epton M, Weckner O, Xu J and Askari E. Peridynamic states and constitutive modeling. *Journal of Elasticity*, Vol. 88, pp 151–184. 2007.
- [6] Diehl P, Prudhomme S and Lévesque M. A review of benchmark experiments for the validation of peridynamics models. *Journal of Peridynamics and Nonlocal Modeling*. 2019.
- [7] Heinecke F and Willberg C. Manufacturing-induced imperfections in composite parts manufactured via automated fiber placement. *Journal of Composite Science*, Vol. 3, No. 2. 2019.
- [8] Bertram A. *Elasticity and plasticity of large deformations (Second Edition): An introduction*. Springer Berlin, Heidelberg. 2008.
- [9] Tupek M R. *Extension of the peridynamic theory of solids for the simulation of materials under extreme loadings*. Ph.D. thesis, Massachusetts Institute of Technology. 2014.
- [10] Breitenfeld M, Geubelle P, Weckner O and Silling S A. Non-ordinary state-based peridynamic analysis of stationary crack problems. *Computer Methods in Applied Mechanics and Engineering*, Vol. 272, pp 233–250. 2014.
- [11] Chen H. Bond-associated deformation gradients for peridynamic correspondence model. *Mechanics Research Communications*, Vol. 90, pp 34–41. 2018.
- [12] Li P, Hao Z and Zhen W. A stabilized non-ordinary state-based peridynamic model. *Computer Methods in Applied Mechanics and Engineering*, Vol. 339, pp 262–280. 2018.
- [13] Tupek M R and Radovitzky R. An extended constitutive correspondence formulation of peridynamics based on nonlinear bond-strain measures. *Journal of the Mechanics and Physics of Solids*, Vol. 65, No. Supplement C, pp 82–92. 2014.
- [14] Wu C. Kinematic constraints in the state-based peridynamics with mixed local/nonlocal gradient approximations. *Computational Mechanics*, Vol. 54, No. 5, pp 1255–1267. 2014.
- [15] Wu C and Ren B. A stabilized non-ordinary state-based peridynamics for the nonlocal ductile material failure analysis in metal machining process. *Computer Methods in Applied Mechanics and Engineering*, Vol. 291, pp 197–215. 2015.
- [16] Wan J, Chen Z, Chu X and Liu H. Improved method for zero-energy mode suppression in peridynamic correspondence model. *Acta Mechanica Sinica*, Vol. 35, pp 1021–1035. 2019.
- [17] Silling S A. Stability of peridynamic correspondence material models and their particle discretizations. *Computer Methods in Applied Mechanics and Engineering*, Vol. 332, pp 42–57. 2017.
- [18] Foster J T, Silling S A and Chen W. An energy based failure criterion for use with peridynamic states. *International Journal for Multiscale Computational Engineering*, Vol. 9, No. 6, pp 675–688. 2011.
- [19] Rädcl M and Willberg C. PeriDoX. GitHub repository. 2018.
- [20] Willberg C, Wiedemann L and Rädcl M. A mode-dependent energy-based damage model for peridynamics and its implementation. *Journal of Mechanics of Materials and Structures*, Vol. 14, No. 2, pp 193–217. 2019.
- [21] Willberg C, Hesse J T and Heinecke F. Peridynamic simulation of a mixed-mode fracture experiment in

PMMA utilizing an adaptive-time stepping for an explicit solver. *Journal of Peridynamics and Nonlocal Modeling*. 2022.

- [22] International A. *Standard test method for measurement of fatigue crack growth rates*. ASTM international. 2011.
- [23] Heinecke F and Wille T. In-situ structural evaluation during the fibre deposition process of composite manufacturing. *CEAS Aeronautical Journal*, Vol. 9, No. 1. 2018.
- [24] Willberg C and Heinecke F. Evaluation of manufacturing deviations of composite materials. *PAMM*, Vol. 20, No. 1, p e202000345. 2021.